

Role of Percolation in the Conductance of Electrolyte-Gated SrTiO₃

Mingyang Li,^{1,2} Tanja Graf,¹ Thomas D. Schladt,¹ Xin Jiang,¹ and Stuart S. P. Parkin^{1,*}

¹IBM Almaden Research Center, San Jose, California, USA

²Department of Physics, Stanford University, Stanford, California, USA

(Received 26 April 2012; published 9 November 2012)

We study the electrolyte-gate-induced conductance at the surface of SrTiO₃(001). We find two distinct transport regimes as a function of gate voltage. At high carrier densities, a percolative metallic state is induced in which, at low temperatures, clear signatures of a Kondo effect are observed. At lower carrier densities, the resistance diverges at low temperatures and can be well described by a 2D variable range hopping model. We postulate that this derives from nonpercolative transport due to inhomogeneous electric fields from imperfectly ordered ions at the electrolyte-oxide interface.

DOI: 10.1103/PhysRevLett.109.196803

PACS numbers: 73.40.-c, 68.47.Gh

Recently, the use of ionic liquids as the gate dielectric in field effect transistor devices has emerged as a useful means to induce novel conducting states in a variety of materials [1–4]. The use of a liquid electrolyte allows for the introduction of much higher charge densities than is possible using conventional dielectrics. Among the materials being studied by this technique, SrTiO₃ (STO) has attracted much attention [1,5,6]. One motivation for these studies is to probe the properties of the two-dimensional electron gas (2DEG) that is formed at the interface between (001) oriented STO and LaAlO₃ (LAO), without the additional complexity of the growth of an oxide interface. Moreover, the use of electrostatic gating allows for the controllable introduction of a range of carrier densities, whereas the 2DEG at the STO(001)/LAO(001) interface is observed to form abruptly when the thickness of the LAO layer is increased above a critical thickness of three unit cells—a phenomenon attributed to the diverging electric field at the interface resulting from the polar nature of the LAO(001) surface [7].

At high carrier densities electrolyte-gated STO is metallic to low temperatures and exhibits superconductivity below ~ 300 mK [1], a similar behavior to that of the 2DEG formed at the STO/LAO interface [8]. However, at lower carrier densities, a striking feature of electrolyte-gated STO is that the resistance is found to increase at low temperatures for a wide range of carrier densities. This has been attributed to various effects such as a metal-insulator phase transition [5] or a Kondo effect [6]. An important factor that has been largely overlooked is the role of disorder. Disorder is known to play a critical role in the transport properties of low-dimensional systems such as various chemically doped oxides [9–11] and semiconductors, as well as metal-oxide-semiconductor (MOS) field effect transistors (FET) [12]. Recent studies have reported the observation of strong localization at the LAO/STO interface for certain growth conditions [13], and the electrolyte-gate-induced conductance at several facets of rutile TiO₂ follows a variable range hopping model at low

temperatures consistent with strong localization [14]. Disorder induced by inhomogeneous electric fields derived by imperfect ordering of the ions in the electrolyte is also likely important [15–17]. In this Letter we demonstrate that electrolyte gating of (001) STO leads to two distinct conductance regimes. At low gate voltages, in a “nonpercolative” regime, the resistance diverges at low temperature and follows a variable range hopping mode [9,18]. In the “percolative” regime, a metallic resistance behavior is observed, but clear signatures of a Kondo effect are found, indicative of the presence of localized spins [5,19].

Figure 1(a) shows a schematic diagram of the device used in this study that was fabricated using standard photolithographic methods. As-received STO (001) single crystalline substrates were treated first with a buffered HF solution and were then annealed at 1000 °C for 90 min in

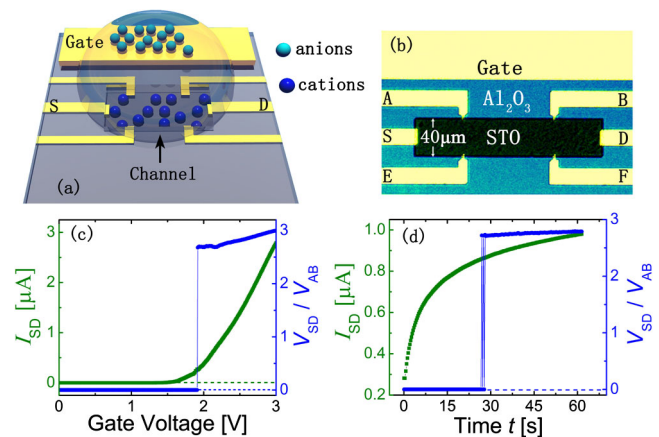


FIG. 1 (color online). (a) Schematic diagram of the device. (b) Optical micrograph of a typical device. (c) Typical I_{SD} versus V_G curve measured by ramping V_G from 0 to 3 V at a rate of 10 mV/s. $V_{SD}/V_{AB} = 0$ corresponds to an open electrical contact between A and B shown in (b). (d) Typical time evolution of I_{SD} and V_{AB} measured after $V_G = 2$ V is applied instantaneously. The dashed lines in (c) and (d) indicate zero values of the ordinates.

an ambient oxygen atmosphere. Atomic force microscopy studies showed that this cleaning method creates surfaces with atomically flat terraces. We used a lateral device configuration with channel dimensions $w = 40 \mu\text{m}$ and $l = 200 \mu\text{m}$, and a large gate electrode measuring $350 \mu\text{m} \times 600 \mu\text{m}$. Contact electrodes (5 nm Ta/65 nm Au) in a Hall bar geometry [Fig. 1(b)] were fabricated by ion beam deposition. Prior to the contact deposition, the STO surface underneath the contact lines was metallized by Ar ion milling for 5 min to minimize contact resistance. A 60 nm thick alumina layer was deposited to define the channel area and to separate the gate electrode from the STO surface. Before each gating experiment, the fabricated devices were treated in vacuum (10^{-7} Torr) at 120°C for 12 h to remove any contaminants resulting from the photolithographic processes. Just prior to the gating experiments, a small droplet of the ionic electrolyte 1-ethyl-3-methylimidazolium bis(trifluoromethylsulfonyl) imide (EMIM-TFSI) was positioned on the device to cover the channel and gate areas. During all our experiments, unless otherwise stated, the voltage V_{SD} between the source and drain [electrodes S and D in Fig. 1(b)] was kept constant at 0.1 V, while the gate voltage V_G applied between the gate and drain contacts was varied. The source-drain current I_{SD} , the voltage drop along the edge of the channel V_{AB} , and the two Hall voltages V_{AE} and V_{BF} were continuously monitored. The leakage current I_G between the gate and the drain remained below ~ 0.1 nA in all of the experiments, indicating that electrochemical processes within the electrolyte were negligible.

When a gate voltage is applied, cations and anions in the electrolyte move towards the corresponding electrodes. An electric double layer (EDL) is formed at the interface between the liquid and the oxide surface. By varying the gate bias in such an electric double layer transistor geometry the amount of charge within the EDL can be continuously tuned. Figure 1(c) shows a typical dependence of I_{SD} on V_G at room temperature, when V_G was ramped up slowly from 0 to 3 V at a rate of 10 mV/s. The channel becomes conducting between S and D after V_G reached a threshold voltage of ~ 1.5 V, which is indicated by a sharp increase of I_{SD} . On the other hand, V_{AB} remained open ($V_{SD}/V_{AB} = 0$) until V_G reached a second threshold voltage of ~ 1.9 V. As shown in Fig. 1(d), a similar behavior was observed when $V_G = 2$ V was applied instantaneously at time zero without slow ramping. The immediate response of I_{SD} indicates the rapid formation of a conducting path between S and D . However, in this particular example, a time delay of ~ 28 sec was observed during which V_{AB} remained open. Moreover, the steady increase of I_{SD} is attributed to the slow redistribution of the electrolyte ions on the STO surface due to low ionic mobility in the liquid. Both the threshold voltage difference and the time delay indicate that the carrier distribution close to threshold is nonuniform across the channel.

Temperature dependent magnetotransport properties were measured in a Physical Property Measurement System (Quantum Design). Because of the slow dynamics in forming the EDL [Fig. 1(d)], and the observed device to device variation, V_G does not presage a certain carrier density at the oxide surface. Instead, a better way to characterize the induced conducting state in STO is given by the steady state current $I_{SD,0}$. Different values of $I_{SD,0}$ were set by applying gate voltages between 1.8 and 2.4 V at $T = 280$ K, and waiting for at least 2 h until the system reached equilibrium. Subsequently, the samples were rapidly cooled to $T = 180$ K at a rate of 5 K/min to freeze the electrolyte in a glassy state. After another equilibration for 30 min, the sample was cooled to $T = 1.8$ K in steps of 0.5 K at a rate of 0.5 K/min. The carrier densities were determined by Hall measurements at $T = 5$ K. The devices returned to their insulating state after warming up and turning off V_G .

Figure 2(a) shows a series of R - T curves under different gating levels. These curves can be well separated into two regimes. We borrow the terminology of the

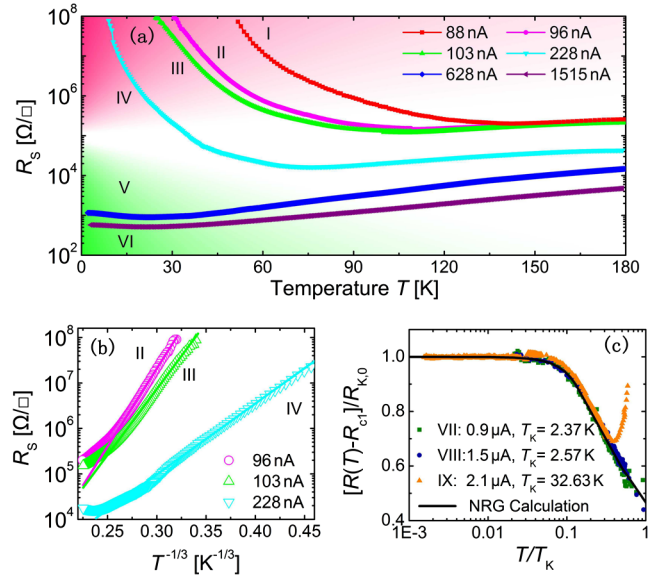


FIG. 2 (color online). (a) Sheet resistivity R_S versus temperature for various gate levels, indicated by the steady state source-drain current $I_{SD,0}$ at $T = 280$ K. The nonpercolative and percolative regimes are shaded in red (upper) and green (lower), respectively. The carrier densities are $2.75 \times 10^{13}/\text{cm}^2$ and $4.31 \times 10^{13}/\text{cm}^2$ for curves V and VI, respectively. The carrier densities for curves I–IV could not be measured because the Hall contacts were open. (b) R_S versus $T^{-1/3}$ for curves II, III, and IV in (a). Solid lines are fits for $T < 50$ K according to a 2D VRH model [i.e., Eq. (1) with $\nu = 1/3$]. (c) Normalized sheet resistance versus temperature (scaled to the corresponding Kondo temperature T_K) for three curves in the percolative regime. The scaling parameters for each curve were determined by fits using Eqs. (2) and (3). T_K varies from 2.37 K to 32.63 K. The solid line was obtained from the numerical renormalization group (NRG) calculations.

random-resistor-tunneling-network (RRTN) model [18] and classify curves I – IV to be in a nonpercolative regime, and curves V and VI to be in a percolative regime. In the latter percolative regime the system exhibits metallic behavior, with a slight increase in resistance at very low temperatures. In the nonpercolative regime, the resistance diverges at $T = 0$ K. We find that the diverging resistance R exhibited by curves II – IV at low temperatures ($T < 50$ K) can be well modeled by a variable range hopping (VRH) model, as follows:

$$R = R_0 \exp\left[\left(\frac{T_0}{T}\right)^\nu\right], \quad (1)$$

where R_0 is a scaling constant, T_0 is a characteristic temperature that depends on details of the model, and the index ν is given by $\nu = 1/(1+d)$ for d -dimensional, noninteracting, strongly localized systems [9], $\nu = 1/2$ for Efros-Shklovskii variable range hopping systems with Coulomb gaps [20], and $\nu = 1$ for band insulators [21]. The optimal fit for curves II – IV yields $\nu = 0.30$ – 0.36 , which favors a 2D VRH model, as displayed in Fig. 2(b). This implies that the diverging resistance in the nonpercolative regime cannot be attributed to a nondegenerate electron gas [1], where the Fermi level lies in the band gap, and which requires $\nu = 1$. In addition, the divergence in resistance is not consistent with a metal-to-insulator phase transition, as has previously been interpreted [5], because, as can be seen from curves I – IV in Fig. 1(a), the resistance increases smoothly with decreasing temperature, rather than abruptly.

The resistance upturns in the percolative regime can be attributed to either a Kondo effect [6] or weak localization [22,23]. To distinguish which effect has the major contribution, we studied the R – T dependence to lower temperatures (20 mK) using a dilution refrigerator. We found that the upturn in resistance saturated at a constant value below a characteristic temperature that depends on gating levels (and thereby the carrier density). This is consistent with the assumption of a Kondo effect. The resistance data were fitted with Eqs. (2) and (3) at very low temperatures ($T \ll T_K$) and intermediate temperatures ($T \sim T_K$), respectively, using the results of numerical renormalization group (NRG) theory [24,25].

$$R(V_G, T) = R_{c1}(V_G) + R_{K,0}(V_G) \left[1 - \frac{\pi^4}{16} \left(\frac{T}{T_K(V_G)} \right)^2 \right], \quad (2)$$

$$R(V_G, T) = R_{c2}(V_G) + \frac{R_{K,0}(V_G)}{2} \left[1 - 0.47 \ln \left(\frac{1.2T}{T_K(V_G)} \right) \right], \quad (3)$$

where T_K is the Kondo temperature, $R_{K,0}$ is the Kondo resistance at $T = 0$ K, and R_{c1} and R_{c2} are temperature independent contributions to the resistance due to other scattering mechanisms. Figure 2(c) shows normalized Kondo resistance versus T/T_K curves, and we find that

all our data for different gate levels fall on one universal curve. This universal Kondo behavior is well described by NRG calculations [24], and therefore provides evidence that the resistance upturns in our experiments are indeed due to the Kondo effect. Two possible origins of the Kondo effect which we observe are (I) the presence of extrinsic magnetic impurities at the surface of the device or (II) intrinsic localized Ti^{3+} states that are induced by the EDL gating. Given the high reproducibility of these upturns for different samples, the latter explanation is more plausible. Moreover, weak magnetization has recently been observed at the LAO/STO interface using highly sensitive torque magnetometry at very low temperatures [26] as well as the $\text{GdTiO}_3/\text{STO}$ interface and in La doped STO [27]. Evidence for a Kondo effect has also been found recently in EDL-gated STO using an ionic gel electrolyte at similar carrier densities [6] (for measurements down to 1.4 K).

The magnetic field dependence was explored in the two transport regimes to gain additional insight into the transport mechanisms. The magnetoconductance (MC) curves at various temperatures are shown in Fig. 3(a) for a nonpercolative case [$I_{SD,0} = 228$ nA, curve IV in Fig. 2(a)]. Contrary to the positive MC predicted [28] in the strong localization regime [13,23], we find a large negative MC that is quadratic in H at low fields. This can be explained by Shklovskii's percolation model [29,30].

$$\ln \frac{\sigma(H)}{\sigma(0)} = -t_1 \frac{e^2 a^4 H^2}{c^2 \hbar^2} \left(\frac{T_0}{T} \right)^{3\nu}, \quad (4)$$

where $t_1 = 0.0028$ for 2D systems [30], ν and T_0 are the same VRH parameters as in Eq. (1), and a is the localization length. Fitting the MC curves using Eq. (4) with parameters ν and T_0 extracted from data in Fig. 2(b), we calculated the localization length a to be 50 Å, which is comparable to reported values in Si MOSFETs [30] and $\text{Ca}_{1+x}\text{Cu}_2\text{O}_3$ films [31].

For comparison, in the percolative regime [$I_{SD,0} = 1515$ nA, curve VI in Fig. 2(a)], a small, negative MC

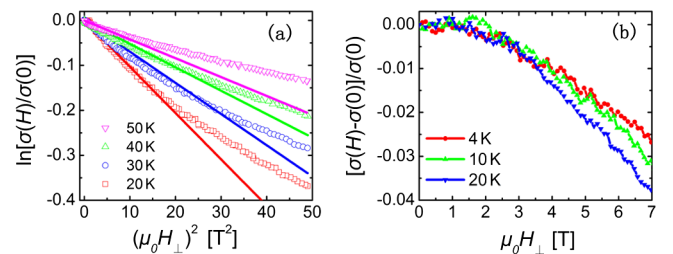


FIG. 3 (color online). (a) $\ln[\sigma(H)/\sigma(0)]$ versus $(\mu_0 H_\perp)^2$ for the nonpercolative curve IV of Fig. 2(a) at various temperatures. Solid lines are fits to the data based on Eq. (4), with $a = 5.0$ nm, $\nu = 1/3$, and $T_0 = 5 \times 10^4$ K. (b) Magnetoconductance for the percolative curve VI of Fig. 2(a) for temperatures between 4 K and 20 K.

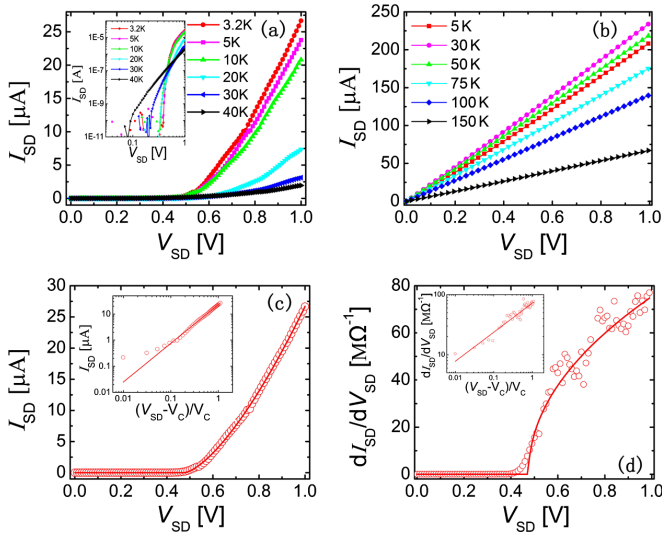


FIG. 4 (color online). (a) I_{SD} - V_{SD} characteristics for a non-percolative curve at temperatures varying from 3.2 K to 40 K. The inset shows the log-log plot of I_{SD} versus V_{SD} . (b) I_{SD} - V_{SD} characteristics for the percolative curve V of Fig. 2(a) at temperatures varying from 5 K to 150 K. (c) The solid line shows the fit to the $T = 3.2$ K data in (a) according to Eq. (5) with parameters $V_C = 0.475$ V and $\delta = 1.48$. The inset shows the corresponding log-log plot. (d) Derivatives of the data and fitted curve in (c) with corresponding log-log plots shown in the inset.

with weak temperature dependence is observed in Fig. 3(b), that most likely derives from Lorentz magnetoresistance effects [6,32]. This is further evidence that the resistance upturn in the percolative regime is not due to weak localization, which would result in a positive MC.

Lastly, we found that in the nonpercolative VRH regime, the device exhibits a nonlinear I_{SD} - V_{SD} response [Fig. 4(a)], as compared to the linear response in the percolative regime [Fig. 4(b)]. The nonlinear I_{SD} - V_{SD} characteristics can be well fitted at low temperatures according to the RRTN percolation model [18,33]:

$$\begin{aligned} I_{SD} &\propto (V_{SD} - V_C)^\delta \quad \text{for } V_{SD} \geq V_C, \\ I_{SD} &= 0 \quad \text{for } V_{SD} < V_C, \end{aligned} \quad (5)$$

where V_C is the macroscopic threshold voltage at which microscopic reversible breakdown takes place within the percolation network and δ is an exponent of the power law dependence. A fit to this model for the $T = 3.2$ K data is shown in Figs. 4(c) and 4(d) and gives $\delta = 1.48$. The deviation of the observed I_{SD} with the model prediction at $V \lesssim V_C$ is due to thermally activated tunneling, which is not included in the model used [Eq. (5)].

Based on our experiments we propose a physical picture for the electrolyte gating effect of STO. When a positive gate voltage is applied, the initially disordered ionic liquid becomes polarized with the formation of a charged layer of cations at the STO surface. The ordering is likely highly imperfect [15], thereby creating an inhomogeneous

electric field within the STO. This will result in local variations in both carrier density and a potential energy landscape. When the gating level is low, metallic regions are disconnected from each other and the conductance is mediated by electrons hopping between these regions, thus leading to a nonpercolative transport regime. As temperature decreases towards zero, the hopping probability diminishes, leading to a diverging resistance. In this regime, a perpendicular magnetic field shrinks the extent of these localized states, and hence decreases the hopping probability, which leads to a large negative MC. The I_{SD} - V_{SD} response is nonlinear due to the tunneling nature of conductance. As the gating level increases, more carriers are created and eventually one or more percolative paths are formed, leading to a metallic behavior of the device, which has a small negative MC and a linear I_{SD} - V_{SD} response. In the percolative regime, localized electrons on Ti^{3+} sites have a magnetic moment which can account for the Kondo effect that we observe. Since similar diverging resistance behaviors at low temperatures have been observed in several other electrolyte-gated systems [2,3,34], we suppose that these results could also arise from percolation effects. We conclude that the effect of disorder resulting from imperfect order in ionic liquid and gels cannot be neglected in electrolyte-gating studies.

T. D. S. thanks the Alexander von Humboldt Foundation for a Feodor Lynen Research Fellowship, and T. G. is supported by the German Science foundation (DFG, GR 4000/1-1). Support from the Graduate School ‘‘Material Science in Mainz’’ (DFG, GSC 266) is gratefully acknowledged. We thank Brian Hughes for help in device fabrication and Wei Han for valuable discussions.

*stuart.parkin@us.ibm.com

- [1] K. Ueno, S. Nakamura, H. Shimotani, A. Ohtomo, N. Kimura, T. Nojima, H. Aoki, Y. Iwasa, and M. Kawasaki, *Nature Mater.* **7**, 855 (2008).
- [2] J. T. Ye, S. Inoue, K. Kobayashi, Y. Kasahara, H. T. Yuan, H. Shimotani, and Y. Iwasa, *Nature Mater.* **9**, 125 (2010).
- [3] K. Ueno, S. Nakamura, H. Shimotani, H. T. Yuan, N. Kimura, T. Nojima, H. Aoki, Y. Iwasa, and M. Kawasaki, *Nature Nanotech.* **6**, 408 (2011).
- [4] S. Ono, N. Minder, Z. Chen, A. Facchetti, and A. F. Morpurgo, *Appl. Phys. Lett.* **97**, 143307 (2010).
- [5] Y. Lee, C. Clement, J. Hellerstedt, J. Kinney, L. Kinnischtzke, X. Leng, S. D. Snyder, and A. M. Goldman, *Phys. Rev. Lett.* **106**, 136809 (2011).
- [6] M. Lee, J. R. Williams, S. Zhang, C. D. Frisbie, and D. Goldhaber-Gordon, *Phys. Rev. Lett.* **107**, 256601 (2011).
- [7] S. Thiel, G. Hammerl, A. Schmehl, C. W. Schneider, and J. Mannhart, *Science* **313**, 1942 (2006).
- [8] N. Reyren *et al.*, *Science* **317**, 1196 (2007).
- [9] N. F. Mott and E. A. Davis, *Electronic Processes in Non-crystalline Materials* (Oxford University Press, Oxford, 1979).

- [10] M. Fäth, S. Freisem, A. A. Menovsky, Y. Tomioka, J. Aarts, and J. A. Mydosh, *Science* **285**, 1540 (1999).
- [11] M. Uehara, S. Mori, C. H. Chen, and S.-W. Cheong, *Nature (London)* **399**, 560 (1999).
- [12] P. A. Lee, *Phys. Rev. Lett.* **53**, 2042 (1984).
- [13] T. Hernandez, C. W. Bark, D. A. Felker, C. B. Eom, and M. S. Rzchowski, *Phys. Rev. B* **85**, 161407(R) (2012).
- [14] T. D. Schladt, T. Graf, M. Li, N. Aetukuri, X. Jiang, M. Samant, and S. S. P. Parkin (to be published).
- [15] M. Mezger *et al.*, *Science* **322**, 424 (2008).
- [16] D. A. Walker, B. Kowalczyk, M. O. de la Cruz, and B. A. Grzybowski, *Nanoscale* **3**, 1316 (2011).
- [17] Y. Xia, W. Xie, P. P. Ruden, and C. D. Frisbie, *Phys. Rev. Lett.* **105**, 036802 (2010).
- [18] *Quantum and Semi-classical Percolation and Breakdown in Disordered Solids*, edited by A. K. Sen, K. K. Bardhan, and B. K. Chakrabarti (Springer, Berlin, 2009).
- [19] J. Kondo, *Prog. Theor. Phys.* **32**, 37 (1964).
- [20] A. L. Efros and B. I. Shklovskii, *J. Phys. C* **8**, L49 (1975).
- [21] J.-J. Kim and H. J. Lee, *Phys. Rev. Lett.* **70**, 2798 (1993).
- [22] P. A. Lee and T. V. Ramakrishnan, *Rev. Mod. Phys.* **57**, 287 (1985).
- [23] S.-Y. Hsu and J. J. M. Valles, *Phys. Rev. Lett.* **74**, 2331 (1995).
- [24] T. A. Costi, A. C. Hewson, and V. Zlatic, *J. Phys. Condens. Matter* **6**, 2519 (1994).
- [25] J.-H. Chen, L. Li, W. G. Cullen, E. D. Williams, and M. S. Fuhrer, *Nat. Phys.* **7**, 535 (2011).
- [26] L. Li, C. Richter, J. Mannhart, and R. C. Ashoori, *Nat. Phys.* **7**, 762 (2011).
- [27] P. Moetakef, J. R. Williams, D. G. Ouellette, A. Kajdos, D. Goldhaber-Gordon, S. J. Allen, and S. Stemmer, [arXiv:1204.1081v1](https://arxiv.org/abs/1204.1081v1).
- [28] U. Sivan, O. Entin-Wohlman, and Y. Imry, *Phys. Rev. Lett.* **60**, 1566 (1988).
- [29] B. I. Shklovskii and A. L. Efros, *Electronic Properties of Doped Semiconductors* (Springer, New York, 1984).
- [30] G. Timp and A. B. Fowler, *Phys. Rev. B* **33**, 4392 (1986).
- [31] K. G. Lisunov, B. Raquet, H. Rakoto, J. M. Broto, E. Arushanov, X. Z. Xu, H. El Alami, and C. D. Cavellin, *J. Appl. Phys.* **94**, 5912 (2003).
- [32] M. Ben Shalom, C. W. Tai, Y. Lereah, M. Sachs, E. Levy, D. Rakhmilevitch, A. Palevski, and Y. Dagan, *Phys. Rev. B* **80**, 140403 (2009).
- [33] A. J. Rimberg, T. R. Ho, and J. Clarke, *Phys. Rev. Lett.* **74**, 4714 (1995).
- [34] H. Shimotani, H. Asanuma, A. Tsukazaki, A. Ohtomo, M. Kawasaki, and Y. Iwasa, *Appl. Phys. Lett.* **91**, 082106 (2007).